JEAN-FRANÇOIS DAIGLE

PROBING CONTAMINATED AEROSOL CLOUDS USING REMOTE FILAMENT INDUCED BREAKDOWN SPECTROSCOPY

Mémoire présenté

à la Faculté des études supérieures de l'Université Laval

dans le cadre du programme de Maîtrise en Physique

pour l'obtention du grade de Maître en Sciences (M.Sc)

DÉPARTEMENT DE PHYSIQUE, GÉNIE PHYSIQUE ET OPTIQUE

FACULTÉ DE SCIENCES ET GÉNIE

UNIVERSITÉ LAVAL

QUÉBEC

2008

Résumé

Une technique de télédétection par spectroscopie de plasma induite par filamentation (R-FIBS pour remote filament-induced breakdown spectroscopy) est utilisée pour sonder un nuage d'aérosols aqueux contenant des sels métalliques en solution. Nous avons démontré expérimentalement que cette technique peut être utilisée efficacement pour caractériser à distance la composition d'un nuage d'aérosols. En effet, la fluorescence caractéristique de tous les ions métalliques a été observée. De plus, ces raies d'émission étroites excitées par un plasma à faible densité ont pu être identifiées simultanément sans recouvrement spectral. Les résultats obtenus démontrent qu'il est possible d'identifier et distinguer simultanément tous les composants métalliques dissous dans un tel nuage. La technique a également été testée avec succès à une distance de 70 m sur un nuage aqueux contenant du chlorure de sodium.

Abstract

Remote Filament Induced Breakdown Spectroscopy (R-FIBS) was used for probing a cloud of aqueous aerosols containing a mixture of dissolved metallic salts. We demonstrated experimentally that it can be used as a sensitive sensing technique to remotely retrieve the composition of microdroplets in clouds located at a distance. In fact, fluorescence from all the metallic ions dissolved was observed. Moreover, these spectrally narrow atomic transitions excited by the low density plasma did not show any signal overlap. These characteristic spectra demonstrate that R-FIBS can be used to simultaneously recognize and distinguish every single metallic constituent dissolved inside such a cloud. The technique has been successfully tested for long range field test of 70 m with an aerosol cloud of droplets containing sodium chloride.

Foreword

Ce mémoire est en parti extrait de deux articles que j'ai composés conjointement avec plusieurs étudiants du laboratoire de M. See Leang Chin (Francis Théberge, Weiwei Liu, Guillaume Méjean, Huailiang Xu, Jens Bernhardt, Ali Azarm, Quan Sun, Yousef Kamali) et certains membres du centre de Recherche et développement pour la défense Canada à Valcartier (Gilles Roy, Pierre Mathieu, Jean-Robert Simard).

Mes confrères du laboratoire de M. Chin m'ont principalement assisté lors de la réalisation des expériences de propagation sur longue distance dans le corridor. Le personnel du centre RDDC-Valcartier a contribué aux expériences en confectionnant la chambre à aérosols qui est utilisée lors des expériences et m'ont apporté des commentaires constructifs lors de la correction des articles que j'ai composés.

Le premier article est intitulé « Long Range Trace Detection in Aqueous Aerosol using Remote Filament-Induced Breakdown Spectroscopy » et est publié Applied Physics B sous la référence **87, 749,** (2007). Les résultats de cet article sont rapportés au troisième chapitre du présent document. Le second article est intitulé « Multi-constituents detection in aqueous aerosol clouds using remote filament induced breakdown spectroscopy » et a été publié dans le journal Optics Communications sous la référence **278, 147,** (2007). Les résultats de cet article sont présentés au quatrième chapitre du présent document et l'introduction de ce mémoire en est fortement inspirée.

Les autres sections de ce mémoire sont des textes originaux dont je suis l'auteur.

This work was partially supported by NSERC, DRDC-Valcartier, Canada Research Chairs, CIPI, CFI, Femtotech and FQRNT.

The technical assistance and dedication of Mr. Mario Martin was really appreciated. Moreover, because of his good sense of humour, we had a lot of fun working in this laboratory.

I would like to thank my research director, M. See Leang Chin whom has given me incredible support for all these years. I have a learnt a lot from him and I shall use this man as an example in my future career.

A special thought to every member of the research group I have had the pleasure to work with. I would therefore say to Huailiang Xu, Yousef Kamali, Ali Azarm, Guillaume Méjean, Jens Bernhardt, Claude Marceau, Qi Luo, Abbas Hosseini, Mehdi Sharifi, Weiwei Liu, Francis Théberge, Patrick Tremblay Simard, Yanping Chen, Feng Liang, Quan Sun, Zhendong Sun, Jean Fillion and Jean-François Gravel, thank you very much for all great discussions and support. This work would have never been achieved without you!

I am sincerely thankful for all the love, dedication and support my tender half, Julie Auger, brought me. I love you sweetheart! I should not forget to thank my parents, Gaston et Danielle, who made so many sacrifices so that I can be where I am now.

Table of Contents

List of Tables

List of figures

1. Introduction

Remote, real-time detection of atmospheric aerosols has become a critical issue for numerous domains. In the environment, the development of global climate models through total characterization of atmospheric clouds cannot be achieved without determining the composition of the water microdroplets and other aerosols (1). On the other hand, all those whose responsibility is related to public safety and security from all points of view, including the militaries, are in need of new techniques to efficiently monitor ambient aerosols that could contain toxic chemical or biological agents (2). So far, limited by the current technology, the first aim is not to be able to identify the probed aerosols, but to give an efficient alarm for potentially dangerous clouds of aerosols as far as possible.

The present work is an attempt to demonstrate that Remote-Filament Induced Breakdown Spectroscopy (R-FIBS) (3) can efficiently be used for remote identification of some aerosol contents in real applications. Our goal is to try to approach the ideal detection performance. An ideal remote detector that could efficiently probe atmospheric aerosols should fulfill the following objectives (4).

1. Possibility of remote detection at variable distances
2. Sensitive to low concentrations
3. Simultaneously detect, recognize and distinguish multiple constituents.

The following justifies the choice of such requirements for practical purposes.

For the first criterion, the tolerated critical distance of detection depends on the targeted application. We will discuss two of them: industrial security and atmospheric meteorology.

The industrial sector is mainly concerned with air monitoring issues to prevent human respiratory intoxications that could lead to unhealthy long-term diseases or immediate death (5; 6) and environmental pollution. Depending on the size of the probed facility, the appropriate range of detection for the industrial applications lies between 20 m and 500 m. For the latter, cloud characterization, atmospheric pollution and acid rain monitoring are few of the many topics of interest where our ideal instrument could bring some answers. In the troposphere, cirrus, cirrocumulus and cirrostratus are the highest clouds reported around 7 km above Earth's surface (7). On the other hand, the lowest clouds, such as nimbostratus, stratus and cumulus, have been reported from 50 m to 2 km above Earth's surface (7). Considering that particulate pollution stays in the lower regions of the troposphere, a detection distance of less than 2 km should be adequate in most applications. The technique proposed in this work has the potential to reach this detection distance.

The second criterion ensures that the obtained results are useful and accurate. For numerous industrial facilities, airborne particulate matter is a major security concern. In fact, mining industry and crude oil tanking often generate particulate matter so toxic that the tolerated concentration in air is roughly few hundreds of micrograms per cubic meter (5; 6; 8) These targeted products have to be constantly and efficiently monitored at all times. Many filter-based instruments (9) can reach these low concentrations, but results come within hours and these techniques are rather time and money consuming. In these conditions, filter-based instruments cannot provide real-time acquisition for constant monitoring. The current work would be able to provide real-time acquisition data.

The last requirement concerns precision of identification. Most of the time, remote sensing

involves unknown airborne particles that contain numerous constituents. An ideal detector's task is to instantaneously detect and recognize, with one single test, every constituent of the probed droplets. However, fluorescence signal overlap is often related to simultaneous measurement of multiple components. In fact, it is possible but not trivial to distinguish spectrally similar signals originating from different constituents of biological material (10) and gaseous mixtures (11) using a similar LIDAR technique as the one used in this work. For the detection of metallic ions dissolved in water aerosols, this difficulty is avoided using R-FIBS because the resulting atomic spectral lines are very narrow and hence easily resolvable.

At short distances, the nanosecond Laser-Induced Breakdown Spectroscopy (ns-LIBS) has proven its feasibility on aqueous calcium aerosols (12). However, it seems very difficult to extend this technique to remote sensing purposes. Indeed, because of diffraction, it becomes unrealistic to deliver enough intensity at a far distance to create a plasma. This limitation can be circumvented by the use of femtosecond terawatt laser pulses. The propagation of such laser pulses in air is dominated by nonlinear effects which result in the formation of a self-guided structure that is called filament. This filament appears as a dynamic equilibrium between Kerr self-focusing and self-defocusing by the self-generated low-density plasma produced by multiphoton/tunnel ionization of the air molecules (13). Moreover, filaments, having a clamped intensity of approximately 5×10^{13} W/cm^2 in air (14) that is high enough to ionize molecules, have been observed as far as 2 km (15). Because the high intensity inside the filament is clamped, the fluorescence signals of molecules inside the filament column are rather uniform throughout the entire filament volume (3; 16; 17). R-FIBS has already demonstrated its efficiency on metallic (3) and solid biological

(11; 18) samples. The Teramobile group demonstrated that on copper and steel targets (3) the detection technique was very promising for kilometer range applications. In addition, terawatt femtosecond laser pulses successfully excited fluorescence from gaseous (16; 19; 20) targets in femto-LIDAR configuration. R-FIBS thus represents an attractive candidate for time resolved remote sensing of atmospheric aerosols constituents.

The Teramobile group also reported several filament-LIDAR applications related to aerosols (21; 22; 23). They showed that, as long as the transmitted power of the whole beam is higher than the critical power, filaments can survive the interaction with aerosols. Another one was especially dedicated to broadband two-photon laser induced fluorescence (LIF) measurements on bioaerosols (24). Recently, Fujii *et al*. demonstrated that sodium atomic lines could be observed using R-FIBS in aerosols (25). The authors focused 160 mJ compressed pulses of 50 fs with a 20 m concave mirror on a thick aerosol target. They were able to detect sodium fluorescence in a cloud of 300 g/L salt concentration positioned 16 m away from the focusing mirror. This concentration roughly corresponds to the concentration of the Dead Sea (26). For regular oceans, the salinity of water is approximately 150 g/L.

In the present work, using a similar technique but with a special focusing telescope that allows the control of filaments at long distances (16), we demonstrated that ppm level sodium can efficiently be excited and observed 70 m away from the detection system. Also, in comparison with the previous study of Fujii *et al.* (25), the threshold for salt concentration is reduced by 4 orders of magnitude. It is interesting to note that, the four main atomic hydrogen spectral bands from the Balmer series were also detected. This indicates that the breakdown of the water droplets into atomic species occurred.

We also demonstrated that it is possible to simultaneously recognize and distinguish

multiple constituents dissolved in water droplets (aerosols). In this case, the solution consisted of a mixture of lead dichloride, copper dichloride, iron dichloride and sodium chloride. The first three items are mainly of interest to mining industry. In fact, these products, especially lead dichloride, are toxic materials and constant respiratory exposure can lead to many related diseases. Also, it is well known that iron dichloride is highly corrosive and that copper dichloride, due to its high solubility in water, is a severe marine pollutant. In our experiment, all the metallic ions dissolved in the aqueous solution were detected, recognized and distinguished from the others. These promising results demonstrate the great potential of the technique.

2. The physics of filamentation

As previously mentionned, filamentation (13) is the result of a dynamic balance between two non linear effects, namely Kerr self focusing and defocusing by a multiphoton/tunnel ionized plasma (27).

The first effect is caused by a modification of the refraction index of the medium, which at high intensities can be expressed as an intensity dependent Taylor series. At low intensities, only the zeroth order is significant and corresponds to a constant refractive index. However, as the intensity increases, the second order (for the electric field) of the Taylor series has to be taken into consideration. The refractive index can now be expressed as:

(1) $$n(I) = n_0 + n_2 I$$

where n_2 corresponds to coefficient of the second order non linear index and I is the laser pulse intensity (28). If the incident laser pulse has a non-uniform (e.g. gaussian) intensity spatial profile, the index variation on the wavefront's plane will make the optical path traveled by the central part longer than the one traveled by the outer section of the laser pulse. Therefore, the medium will act as a converging lens and will focus the incoming laser pulse. Let us now introduce the pulse's critical power P_{crit} at which the Kerr lens perfectly compensates the defocusing effect caused by linear diffraction:

(2) $$P_{crit} = \frac{3.77\lambda^2}{8\pi n_0 n_2}$$

If the laser pulse power is higher than P_{crit}, it will start to self focus under the action of the Kerr lens. However, this cannot be modeled as a conventionnal linear lens. In, fact, as it is focused, the pulse intensity will increase and the Kerr lens becomes stronger causing a refactive index gradient along the propagation axis. As opposed to a conventional lens, the Kerr lens will constantly increase the rate of change of the wavefront's curvature. Therefore, it can be considered as being a non linear quadratic lens whose focusing power is dependent on the incident intensity. Considering a hypothetical case where no other effect would be present to limit this behavior, the entire beam energy would be focused into a singularity leading to a 'catastrophic collapse'.

However, in our real material world, this catastrophy is avoided by higher order non linear effects which come into play when the intensity around the beam center becomes excessively high. These high intensities will produce ionization of the medium through multiphoton/tunnel ionization. At 800 nm, 8 and 11 photons are required to ionize O_2 and N_2 respectively. This ionization requires laser intensities of the order of 10^{13}-10^{14} W/cm^2. The fast ionization of the medium leads to the formation of a plasma column along the laser beam path. The generated plasma will make the refractive index of the medium smaller than unity and will tend to defocus the laser pulse. Therefore, the defocusing plasma generated inside the medium will balance the Kerr self focusing effect and lead to the formation of a low plasma density ($N_e \approx 10^{16}$ cm^{-3}) structure called filament.

A single filament can extend over distances up to several hundreds of meters; more than 10000 times the Rayleigh range for linear propagation. Two major models have been developped to explain this phenomenon, namely:

- Self guiding of the light where the Kerr effect and plasma defocusing combine to form a structure similar to a waveguide which consists of a weakly ionized core surrounded by a higher refractive index cladding (29; 30).

- The moving focus theory which relies on the non uniform temporal intensity profile of the laser pulse. In this scenario, due to their respective power, the different temporal slices are focused at different distances and give rise to the perception of a filament (31).

For these two models, filamentation starts with Kerr self focusing. Once the intensity is sufficiently high to ionize the medium, the laser pulse tends to defocus due to the self generated plasma. Then, the beam diameter increases and if the power is still higher than P_{crit}, the self focusing effect takes over for another cycle. However, even if the two models have similarities, the moving focus scenario seems to be more appropriate. In fact, without any external focusing, the self focusing distance z_f is governed by the Marburger formula (32):

$$z_f = \frac{0.367ka^2}{\left\{\left[\left(\frac{P}{P_{crit}}\right)^{1/2} - 0.852\right]^2 - 0.0219\right\}^{1/2}} \quad (3)$$

Where ka^2 indicates the diffraction length, k is the wave number, a is the radius at $1/e^2$ level of the beam profile and P is the power of the pulse slice. Because of the pulse's non uniform temporal

intensity, the self focusing distance of the various slices will be dependent on their respective power. This gives the perception of a filament. In the case of external focusing using a lens of focal length *f* the position of the self-focus will change to:

(4)
$$z_f' = \frac{z_f f}{z_f + f}$$

The filament length is L= $f - z_f'$. Any refocusing after the geometrical focus is neglected because the intensity would be weaker in the re-focusing zone.

Since the filaments survive only through ionization of the medium in which they propagate, they can be used to remotely sense an unknown transparent medium. In fact, recombination of the plasma with the ions will produce fluorescence which constitutes a fingerprint of the ionized medium. Filaments therefore allow remote identification of a medium (gases, metallic, biological, aerosols) and as we will see later on, their unique properties are ideal for long distance remote sensing.

The defocusing property of the plasma generated inside the medium where the laser pulse propagates limits and stabilizes the filament's intensity. In fact, it is fixed at a value sufficiently high to generate the plasma that has the appropriate density to start the defocusing process. Therefore, as long as the filament survives, its intensity will be kept constant along its propagation axis. We thus say that the intensity inside a filament is clamped. In air, it is clamped at a value of 5×10^{13} W/cm^2 (14).

3. Towards optimal filamentation control for remote sensing purposes

Filamentation intensity clamping represents an incredible advantage for remote sensing purposes. In linear regimes, diffraction limits the intensity that can be delievered around the focal point of any focusing device. The beam diameter will linearly increase with the focal distance following the relation:

$$\Delta\varphi = f\lambda/\pi D \tag{5}$$

where $\Delta\varphi$ is the focal diameter, f is the effective focal length of the device, λ is the wavelength of the incident light and D is the input beam diameter. Thus, the intensity around the focal plane of two 10 J/10 ns/ 532 nm laser pulses each focused at 500 m and 1 km is respectively limited at 5×10^{10} W/cm^2 and 1.2×10^{10} W/cm^2. This intensity will continue to go down with an increasing focal length. On the other hand, the filament's clamped intensity (5×10^{13} W/cm^2) provides non diffraction limited interaction zone for ionization of constant and uniform intensity throughout its entire volume, no matter the focusing distance and the pulse duration/energy. Therefore, the backscattered fluorescence signals of the ionized region will not be dependent on the focusing distance and the detected signal will mainly depend on the solid angle.

This is true as far as single filaments are concerned. When we need to increase the return signals from a remote target excited by the filaments of a laser pulse, the energy of the pulse is increased to enhance the excitation. Theoretically, with a perfectly gaussian wavefront, the increasing energy leads to the single filament elongation. However, high power laser pulses emitted from an amplifier have relatively large diameters to avoid any damage to the compressor's grating. Thus, an increase in the pulse energy will tend to

deteriorate the quality of the intensity spatial profile. The hot zones generated will each tend to self-focus into a filament. This is the phenomenon of multiple filamentation (33). Multiple filaments that result from such relatively large diameter pulses will compete for the energy inside the limited reservoir of the pulse leading to many low plasma density structures inefficient for remote sensing purposes. In fact, it is now recognized that filament competition will lead to random and relatively weak return signal from the target (33).

A technique to avoid or minimize this competition is to reduce the diameter of the beam (34) such that when they self focus, the various hot zones will 'cooperate' and the electric field distribution of and around each filament will undergo constructive interference with the others. This interference occurs because the filaments' zones are now very close to one another. This idea was indeed proven valid and the signal was increased by more than three orders of magnitude by reducing the laser pulse's diameter by about three times (34). However, in this case, filamentation started rather early and the self-focusing position could not be changed naturally by increasing the negative chirp or the beam divergence. This is because when the laser beam diameter is 'squeezed' down, the hot zones' diameters are also reduced and forced together around the beam center. According to eq. (3), a smaller diameter hot zone would lead to a shorter self-focal distance which results in early filamentation at short distances making remote detection a hard task.

A device to move the filament zone was then designed by using the combination of beam expansion and geometrical focusing. This device is described in reference (16). From eq.

(3), when the beam is expanded, the diameter/size of the hot zone in the beam cross section becomes larger which in turn, increases the self-focusing distance. The beam diameter could in principle be made very large; hence, the self-focusing distance of each hot zone could become very far. We now use a focusing element to force the beam energy to converge towards the geometrical focus. The focal distance of the device is made shorter than the hot zones' self-focusing distance. Thus, the combination of self-focusing and geometrical focusing will bring the self-focal zones (filaments) to the position in front of or right next to the geometrical focal zone or the Rayleigh range. This is equivalent to squeezing the beam diameter in front of the geometrical focal region to enhance constructive interference among the various filaments. This high intensity zone will then strongly interact with any medium to create a plasma and fluorescence signals.

The device consists of a 5 cm diameter convex mirror, whose focal length is −50 cm, and a focusing lens with focal length of 100 cm (diameter of 8 cm). The focusing lens was installed on a computer-controlled motorized stage, allowing us to change the telescope's effective focal length. Its purpose consists in generating high plasma density filaments at a far distance with a minimum of white light generated through self-phase modulation and self-steepening (35). In order to counter the unwanted effects of multi filamentation energy competition, the hot spots are stretched by increasing the beam diameter with the convex mirror. As previously explained, the larger beam diameter leads to an increased self focusing distance. The converging lens' power is adjusted to make sure that the geometrical focusing distance is much smaller that the free propagation self-focusing distance. Indeed, from equation (4), if z_f is much larger than f, the self focusing position z_f^i

is approximately equal to f. This means that all the energy contained inside the filaments are merged around the geometrical focusing area. This focusing device is the cause of all the following successful results.

4. Long Range Trace Detection in Aqueous Aerosol using Remote Filament-Induced Breakdown Spectroscopy

In the present work, using a similar technique as in reference (25) but with our specially designed beam sending device that allows the control of filaments at long distances (16), we demonstrated that ppm level sodium can efficiently be excited and observed in an aerosol cloud located 70 m away from the detection system. Also, in comparison with the previous study of Fujii *et al.* (25), the threshold for salt concentration is reduced by 4 orders of magnitude. It is interesting to note that, the four main atomic hydrogen spectral bands (36) from the Balmer series were also detected. This indicates that the breakdown of the water droplets into atomic species occurred. This latter observation and the capability to detect diluted species inside the aerosol to ppm levels strongly increase the potential of R-FIBS for aerosol detection.

The experiments were performed with the setups shown in figure 1a. Laser pulses, centered at 800 nm, were emitted with a 10 Hz repetition rate by a CPA Ti:Sapphire laser system. They were focused, using our specially designed beam sending device discussed in the previous section (16). The pulse duration could be varied by changing the distance between the compressor's grating pair and the pulse energy is adjusted with a half-wave plate and polarizer.

The aerosols were generated in the same way as Fujii *et al*. (25) by using a commercial ultrasonic humidifier (Sunbeam, Health at home) and injected in a mobile aerosol chamber.

The aqueous solution is made from a de-ionized water solvent in which the appropriate quantity of salt is added. Since the droplet size generated by a similar aerosol source has been measured by Fujii *et al.* (25), we assume that our droplets also have a mean radius of 5 μm. In the first part of the experiments, a 75 cm open ended cylindrical plastic pipe, used as a concentrator, is placed inside the chamber to increase the droplet density. The aerosols traveled from the humidifier to the plastic pipe via a flexible canalization. In order to avoid laser beam scattering by the droplets before the target, an 8 cm diameter ventilator, located just below the entrance of the pipe, blows the excess aerosol leaving the plastic pipe away from the laser path (Fig. 1a). It ensured that, at the entrance of the pipe, the laser pulse would interact with a practically flat and thick aerosol fog. In these conditions, the cloud's optical density is characterized by the complete attenuation of a continuous wave 15 mW He-Ne laser propagating over 75 cm. Later, to demonstrate the feasibility for real atmospheric applications, the droplet concentration is decreased by removing the plastic pipe. In this case, the He-Ne laser transmission, propagating over 120 cm, is 95%. This roughly corresponds to a droplet concentration of 300 cm^{-3} which is approximately 3 times the concentration of the thinnest natural cloud (37). At all times, in order to avoid laboratory contamination, a flexible plastic pipe connects the chamber to a fume hood and sucks the aerosol away. The negative pressure inside the chamber prevented the exceeding aerosol from escaping the chamber into the laboratory.

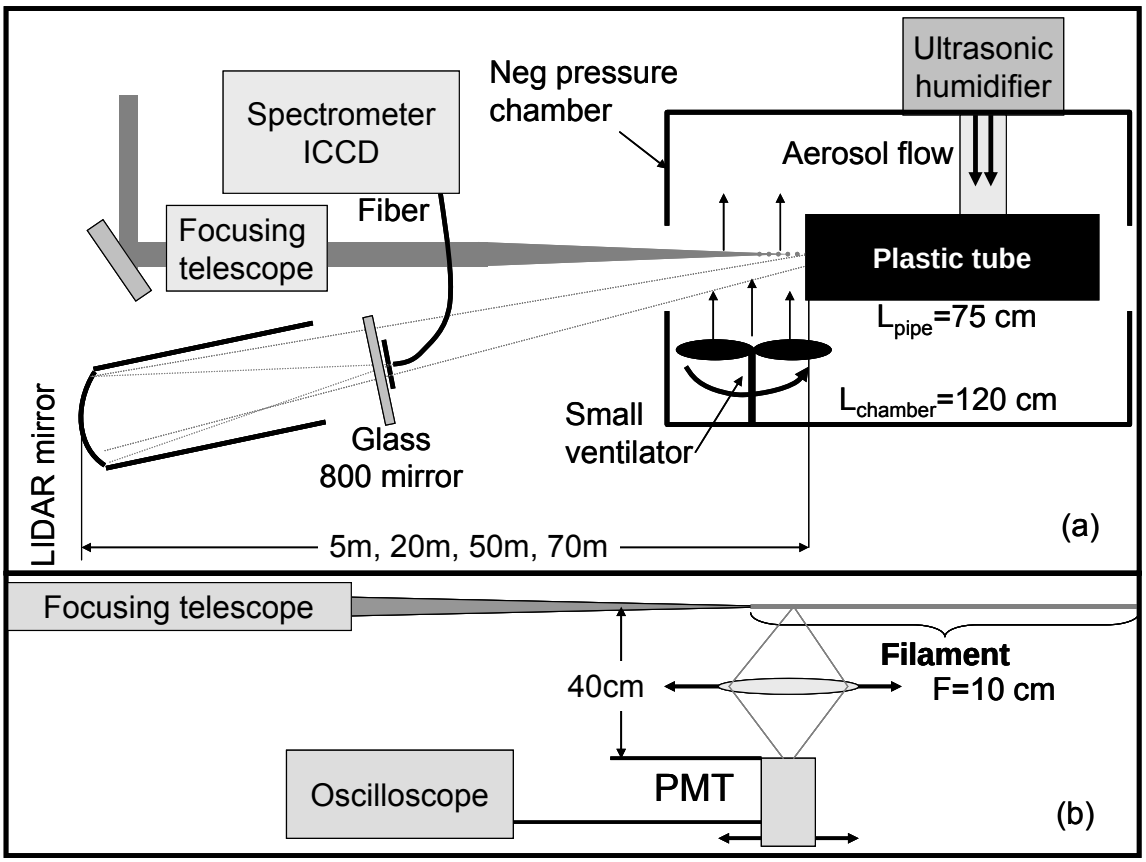

Figure 1: Experimental setups for (a) spectral characterization of aerosols and (b) filament side characterization via molecular nitrogen fluorescence.

In the experiment, the aerosol chamber was located at different distances (5 m to 70 m) away from the sending telescope (Fig. 1a). Beside the telescope, a typical UV fibre coupled LIDAR setup (16) collected the R-FIBS spectra. The 1.5 m focal length LIDAR mirror has 28 cm diameter. The collected signal was delivered to a SpectraPro-500i SP-558 spectrometer equipped with a PIMAX:512 ICCD camera. For each experimental condition, the Na fluorescence signal was optimized by adjusting the effective focal length of the beam delivering device (16).

To show that the interaction with the aerosol involves filamentation, we measured the

nitrogen fluorescence typically emitted from inside a filament (38). Figure 1b shows the experimental set up. For this part of the experiment, the aerosol chamber was removed. A scanning unit, consisting of a fused silica 10 cm focal length lens and a PMT with UG11 filter in a one to one imaging configuration, was moved parallel to the direction of the filament to measure the nitrogen fluorescence distribution from inside the filament as a function of the distance from the LIDAR's output mirror. The distance between the PMT and the filament was 40 cm.

The spectrum presented in figure 2 is the result of 100 shots accumulation. It was measured in thick fog conditions, which means that the pipe was inside the chamber. The corresponding laser pulse duration was negatively chirped to 80 fs with 70 mJ pulse energy. The distance from the pipe entrance to the last lens of the focusing telescope was 3.5 m and 5 m to the LIDAR mirror. The gate of ICCD camera was opened for 500 ns, 8 ns after the laser pulse had arrived at the pipe entrance. In addition to the strong sodium fluorescence, we observed, for the first time in an aerosol cloud, the presence of the four main atomic hydrogen fluorescence bands of the Balmer series which are the result of 7 atomic transitions (36). The first H I-α line is very strong while the rest of the lines are rather weak. These Balmer series proves that the laser pulses induce breakdown of the droplets and H_2O molecules. The fact that the aqueous medium can be detected opens up a way for solvent identification. The plot presented as the inset of figure 2 shows the results obtained using the filament scanning setup shown in figure 1b. The solid line indicates the position of the aerosol pipe entrance. It shows a ~ 50 cm long plasma column penetrating into the pipe for 20 cm. This firmly indicates that the interaction involved filamentation. The

characteristic plasma distribution of the filament shows two spatially separated nitrogen fluorescence signals. Because of the very high input peak power (850 GW after sending telescope), this phenomenon is related to refocusing (39) as well as multiple filamentation (33).

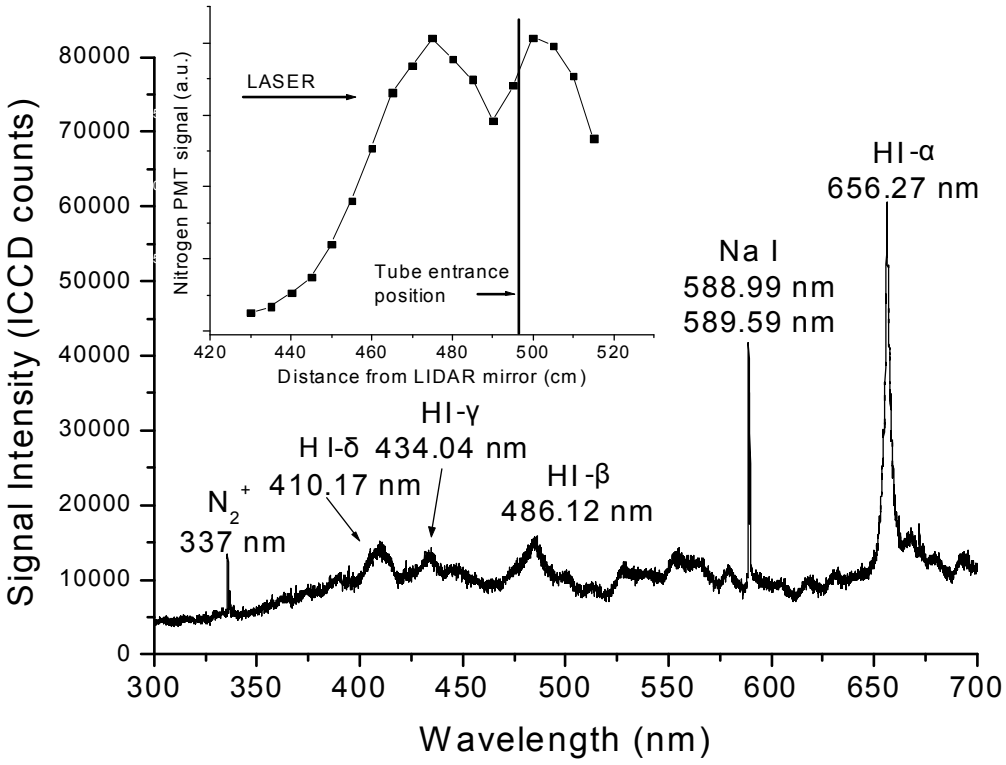

Figure 2: Typical spectrum measured 5 m from the LIDAR mirror with 80 fs negatively chirped pulses of 72 mJ. Inset: Filament generated plasma distribution position with respect to aerosol pipe entrance.

Figure 3 shows the effect of pulse duration on the two major spectral lines. Both sodium and hydrogen emissions increase with pulse duration. This implies that, in order to enhance fluorescence signals, longer pulses are required to heat and accelerate electrons through inverse bremsstrahlung effect. Due to this acceleration, avalanche ionization (27) occurs and produces water droplet breakdown. While transform limited pulses of 47 fs could

excite rather strong sodium fluorescence, longer pulses are needed to excite hydrogen lines. This means that avalanche ionization's involvement in the fluorescence mechanism for hydrogen is more important than for sodium. However, it was found that, for both systems, the signal increased with pulse duration up to a certain limit, which is similar in the cases of both sodium and hydrogen (~80 fs), and then decreases for longer negative chirp. In fact, pulses with longer durations have lower peak powers. Such pulses generate a smaller number of filaments. Since, in our experiment, fluorescence is induced by filamentation, a decrease in the number of filaments reduces the number of water droplets' breakdown events resulting in a weaker R-FIBS signal. This suggests that the optimum aerosol interaction seems to be a compromise between longer pulses avalanche ionization and multiple filamentation from high peak power pulses.

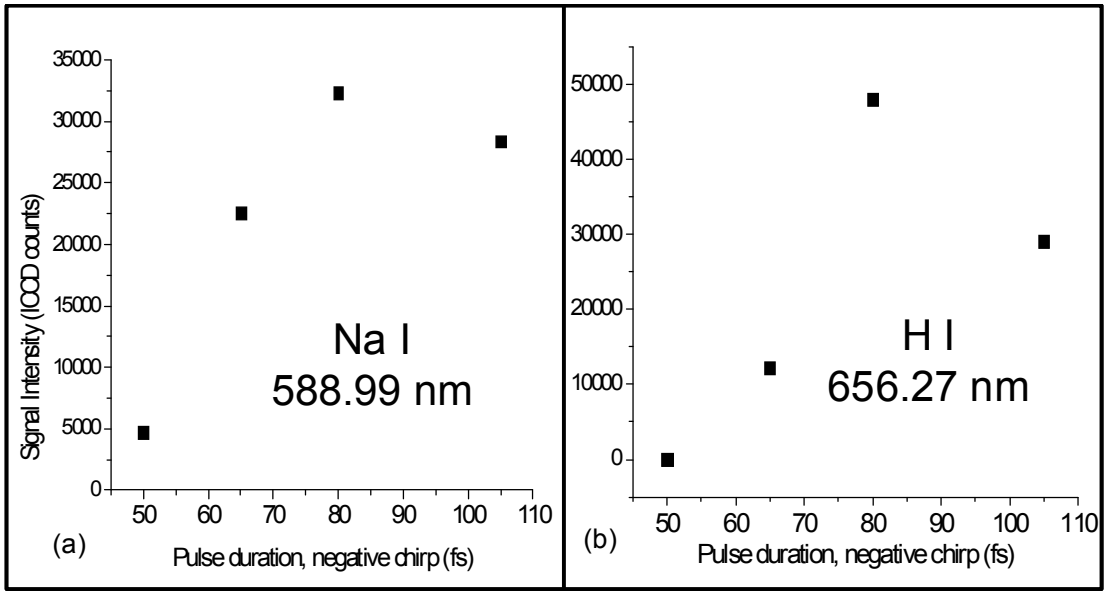

Figure 3: (a) Sodium signal intensity as a function of negative chirp at 5m. (b) Hydrogen signal intensity as a function of negative chirp at 5m.

At 5 m, we measured the detection limit of this technique. First of all, with 70 mJ

compressed pulse energy, the signal could be observed at a salt concentration as low as 7 mg/L (7ppm). As shown in figure 4a, a linear extrapolation to the 3σ level (where σ is the standard deviation of the signal), demonstrates that the detection limit is inferior to 3 ppm. Secondly, at a concentration of 300 mg/L, sodium fingerprint fluorescence could be distinguished with 80 fs chirped pulses of 5 mJ each (figure 4b). In fact, below this energy, it was impossible to generate strong filaments.

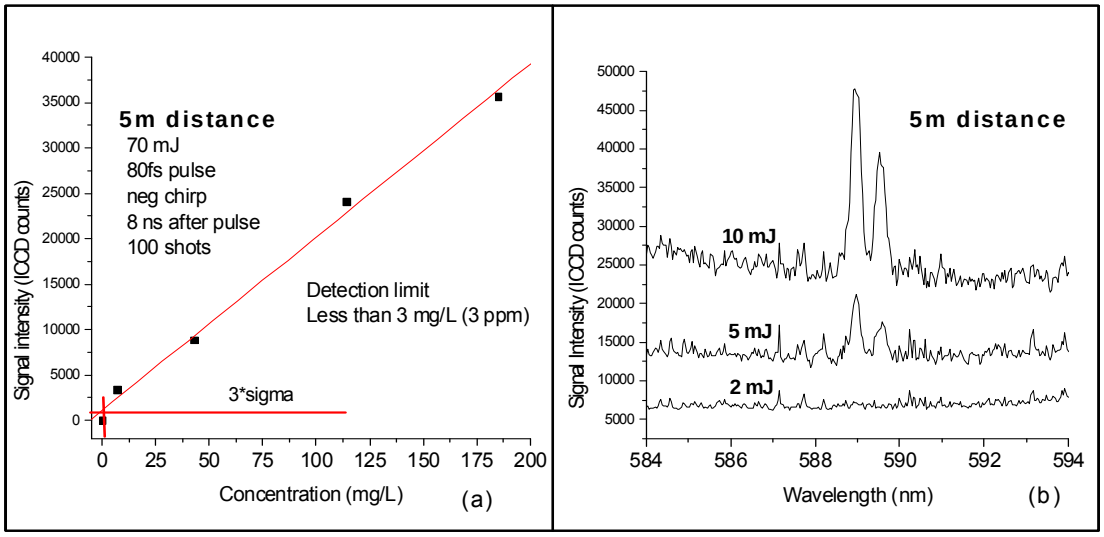

Figure 4: (a) Sodium signal intensity as a function of salt concentration at 5m. (b) Low energy sodium excitation.

The plastic pipe was removed from the chamber and the droplet concentration was characterized with a 95% transmission of the He-Ne laser. Under this condition, the lowest salt concentration at which the sodium lines could be observed, with 70 mJ pulses, was 10 mg/L. When the salt concentration was increased to 20 g/L, two other atomic sodium lines were observed at 568.263 nm and 568.821 nm (36). Finally, 300 mg/L of salt can still be detected with 10 mJ pulses.

Using the same setup as in figure 1a with the plastic pipe in place, we performed the manipulations in a corridor next to the laboratory. Three different chamber positions were considered: 20 m, 50 m and 70 m from the LIDAR mirror. A 5 g/L salt solution was used. . In order to avoid early filamentation in the 10 m tube linking the corridor to the laboratory, negatively chirped 10 ps/72 mJ pulses were launched. Because of the lower peak power (6.8 GW after the sending telescope), the long pulse duration used in this configuration made impossible the observation of the hydrogen lines, even at 20 m. The signal intensity plotted in figure 5 as a function of distance reveals that, at 70 m, the signal is still above the 3σ limit and the lines are easily distinguished from the background (inset of figure 5). Even if the sending telescope's property of generating short and intense filaments cannot be questioned at small distances, the lack of large focusing optics to further increase the beam size for long propagation reduced the sodium detection efficiency. In fact, since the self-focusing distance is proportional to the square of the beam diameter (32), at long focusing ranges, the distance between the geometrical focus and self focus point is reduced. This effect reduces the constructive interference of the multiple filaments which in turn reduces the ionization efficiency. As a result, in addition to the classical $1/R^2$ solid angle factor, the captured signal intensity was influenced by the decrease of filaments plasma density with increasing focal length of the beam delievering device (16). In our experiments, sodium was detected from up to 70m away from the LIDAR. In principle, it is possible to generate intense filaments at km range based upon the current telescopic design (16). This will thus help pushing R-FIBS to km range remote detection.

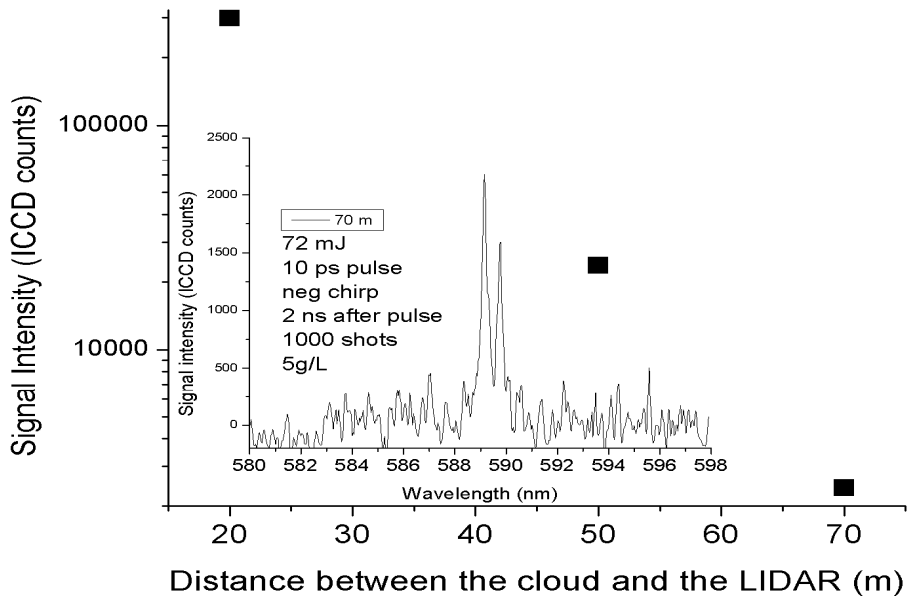

Figure 5: Sodium signal as a function of distance from the LIDAR mirror. Inset: Sodium signal captured with the aerosol chamber positioned 70 m from the LIDAR mirror.

The mobile chamber was then positioned 50 m away from the LIDAR. The salt concentration was gradually decreased to test the detection limit. The results are presented in figure 6. The linear behavior allows the determination of the 3σ detection limit. It was found that, at 50 m, the limit is around 33 ppm which is roughly 10 times larger than at 5 m. This result demonstrates the great potential of the technique for long distance trace measurements in aqueous aerosols.

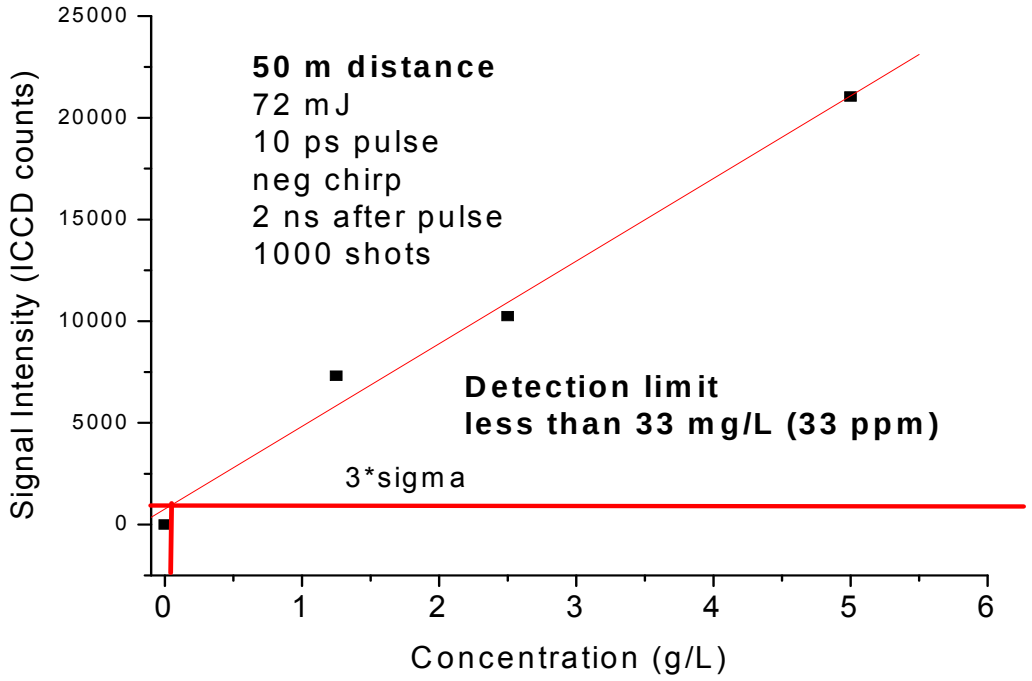

Figure 6: Fluorescence signal as a function of salt concentration at 50m.

Finally, sodium fluorescence from a thin fog characterized with 86% transmission of He-Ne laser and a salt concentration of 1.25 g/L is measured with the chamber positioned 50 m away from the LIDAR mirror. This value of the transmission of He-Ne laser indicates that the droplet concentration is roughly 1000 cm^{-3} (37). It has been reported that filaments can transmit through clouds of optical thickness of up to 3.2 (22). This value has been measured over 0.35 m aerosol fog using He-Ne laser transmission and corresponds to a cloud of droplet density of the orders of 10^5 cm^{-3}. They also concluded that the femtosecond laser pulses can propagate unaffected through a cloud of optical thickness of 1.2 for 0.35 m and still generate filaments (23). In our experiment, the He-Ne laser is transmitted at 86 % and thus, filaments can penetrate the cloud and excite the sodium

fluorescence. In these conditions, unlike thick clouds, at which only a small portion of the filaments interacted with the aerosols, the signal now comes from the entire filament length. The amount of fluorescence captured increases with the size of the interaction volume. So, in thin clouds, filament transmission would lead to enhanced R-FIBS signal.

Because of the above mentioned argument (23), the measured thin fog signal is used to make an extrapolation over distance. Our calibration point is the signal measured from 50 m away under the following conditions: salt concentration, 1.25 g/L; He-Ne laser transmission, 86%; filament length, 1.5 m and 1000 laser shots accumulation. In these conditions, the spectrum is shown as the inset for figure 7. The signal concentration dependence plot in figure 6 and the LIDAR equation $I \propto L/R^2$ (where I is the signal intensity, L the effective filament length and R the distance between the end of the filament and the detector) is used to extrapolate this result over distance. We estimate that, for a filament length of $L = 20$ m, the signal detection limit of 3 standard deviations will be reached, with 10000 shots accumulation, slightly beyond 1.25 km. The extrapolated curve is shown in figure 7 where the black dot represents the calibration point. It is possible to generate such a filament at these distances. However, to achieve this kilometer range detection limit requires control over the onset of the filaments. As previously mentioned, this obstacle could be circumvented using an appropriate telescopic system as a beam focusing device (16). Since the closest clouds, Cumulus humilis, are located around 500-1000 m over sea level (40), this result opens a way for efficient ppm level remote sensing of atmospheric aerosols in air.

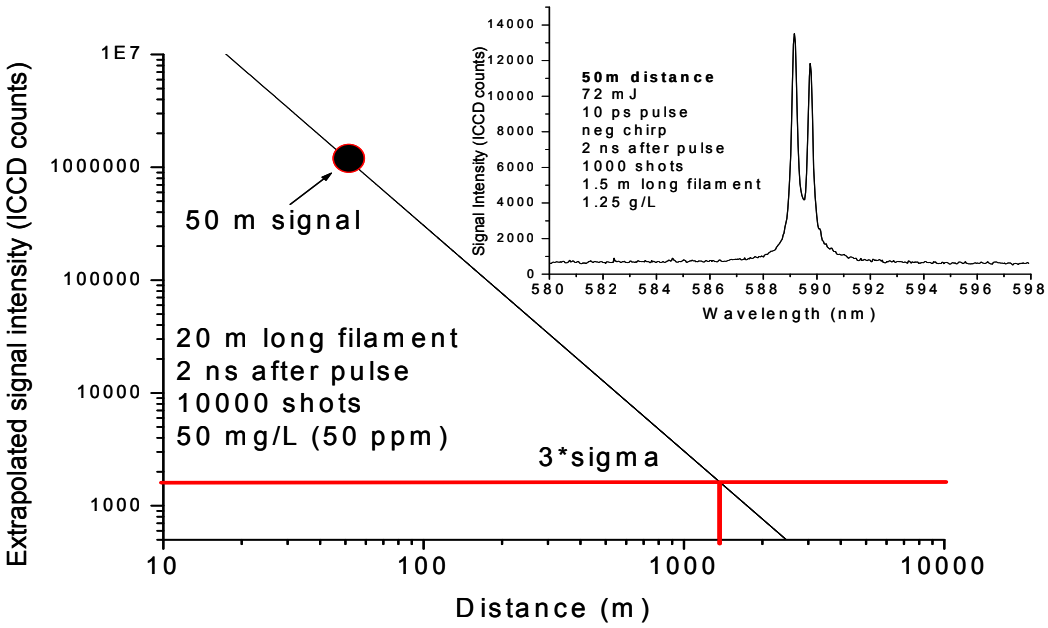

Figure 7: Extrapolation on distance based on a signal collected from a thin cloud at 50 m. Inset: Thin cloud signal at 50 m used for the extrapolation.

Before ending this section, we would like to comment upon the strong discrepancy between these results and those obtained by Fujii *et al.* (25). There was essentially no difference between our experiment and that of Fujii except that we used a specially designed laser beam sending device. In our experiment, with half the pulse energy and a salt concentration lowered by 60 times, approximately the same signal was recovered, but at a distance more than 3 times longer. It appears that, at high energies, in the case of Fujii *et al*, beam profile inhomogeneity and early self-focusing conditions lead to multi-filamentation competition (33) which in turn, decreases the breakdown efficiency. The filaments obtained in the present experiment were, thanks to the focusing device, forced into tight bundle and interfered constructively. In fact, a beam profile analysis showed that, at 20 m, the multiple filaments were confined to a 3 mm minimal diameter high intensity zone around the non-linear focal point.

5. Multi-Constituents Detection in Contaminated Aerosol Clouds using Remote Filament-Induced Breakdown Spectroscopy

The previous series of experiments with sodium demonstrated that it is possible to detect and identify, at a distance of several tens of meters, a single component dissolved at low concentration in a cloud of aerosol droplets. For this experiment, using the same setup as shown in figure 1a, other components were simultaneously dissolved in the droplets. We demonstrate that it is possible to simultaneously recognize and distinguish multiple constituents dissolved in water droplets (aerosols). The solution consisted of a mixture of lead dichloride, copper dichloride, iron dichloride and sodium chloride. The first three items are mainly of interest to mining industry. In fact, these products, especially lead dichloride, are toxic materials and constant respiratory exposure can lead to many related diseases (5; 6; 8). Also, it is well known that iron dichloride is highly corrosive and that copper dichloride, due to its high solubility in water, is a severe marine pollutant. In our experiment, all the metallic ions dissolved in the aqueous solution were detected, recognized and distinguished from the others. This promising result demonstrates the great potential of the technique.

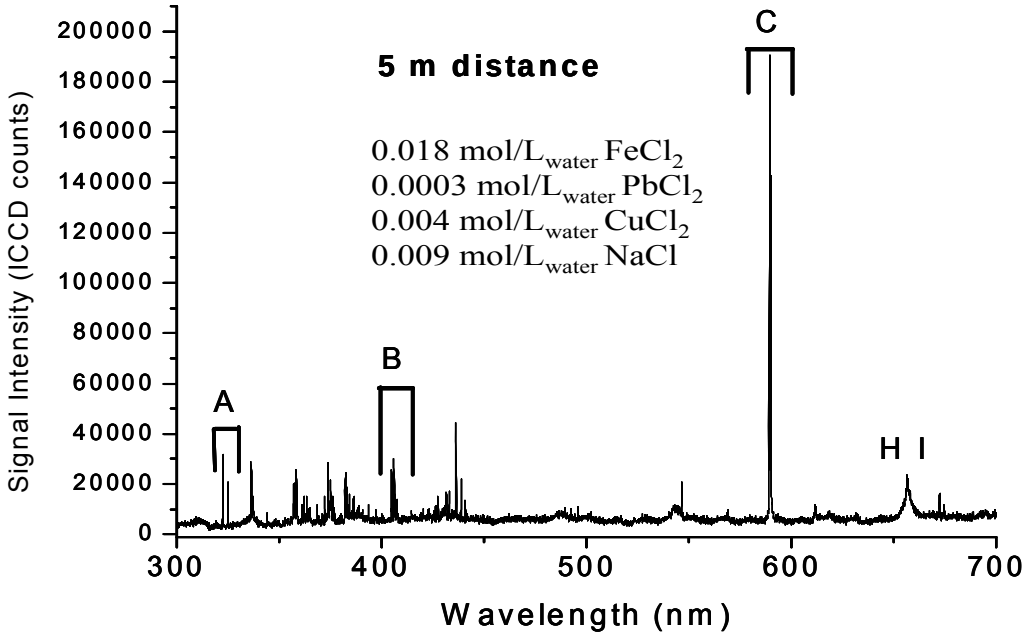

Figure 8: Typical R-FIBS spectrum of a thin aerosol cloud with a 95 % transmission of the 632 nm wavelength containing the listed quantities of iron dichloride, lead dichloride, copper dichloride and sodium chloride.

The experiments were performed with the same setup as the one previously used for our experiments on sodium. The spectrum presented in figure 8 is the result of 160 shots accumulation. The corresponding laser pulse duration was negatively chirped to 500 fs with 51 mJ compressed pulse energy. The de-ionized water solution contained $FeCl_2$, $PbCl_2$, $CuCl_2$ and NaCl at respective concentrations of 0.018 mol/L_{water} (2.25 g/L_{water}), 0.0003 mol/L_{water} (0.9 g/L_{water}), 0.004 mol/L_{water} (0.5 g/L_{water}) and 0.009 mol/L_{water} (0.5 g/L_{water}). Here, in order to produce results in terms of number of ions (independent of the material), molar notations will be used to characterize the various concentrations. The distance from the chamber's entrance was 3.5 m and 5.0 m to the last lens of the focusing telescope and the LIDAR mirror, respectively. The gate of the ICCD camera was opened for 1 ms, 5 ns after the laser pulse had arrived at the cloud layer. In addition to the strong sodium

fluorescence at 589 nm and the main atomic hydrogen fluorescence bands of the Balmer series (36) previously observed in our experiments, the strongest Cu I, Fe I and Pb I lines in the range from 300 nm to 700 nm were detected (36). All the atomic lines observed are listed in table 1.

Fe I	349.05 nm	Fe I	382.58 nm
Fe I	356.54 nm	Fe I	382.78 nm
Pb I	357.27 nm	Fe I	383.42 nm
Fe I	360.89 nm	Fe I	384.10 nm
Fe I	361.88 nm	Fe I	385.99 nm
Fe I	363.15 nm	Fe I	404.58 nm
Pb I	363.96 nm	Pb I	405.78 nm
Fe I	364.68 nm	Fe I	406.35 nm
Pb I	367.15 nm	Fe I	407.17 nm
Pb I	368.35 nm	Fe I	427.17 nm
Fe I	371.99 nm	Fe I	430.79 nm
Fe I	373.49 nm	Fe I	432.57 nm
Fe I	373.71 nm	Fe I	438.35 nm
Pb I	373.99 nm	Fe I	440.47 nm
Fe I	374.95 nm	Fe I	441.51 nm
Fe I	375.82 nm	H I	486.13 nm
Fe I	376.38 nm	Na I	588.99 nm
Fe I	381.58 nm	Na I	589.59 nm
Fe I	382.04 nm	H I	656.27 nm
Fe I	382.43 nm	H I	656.28 nm
Fe I	382.44 nm		

Table 1: List of the atomic spectral components

In figure 9, the regions A, B and C shown in Fig. 8 are enlarged. Regions A and C clearly show that, when these four salts are mixed together, Cu I and Na I emissions can easily be distinguished from the background and from the other materials. Figure 9B shows the selected region for Fe I and Pb I. Three Fe I and one Pb I peaks are observed. It is clear that under these conditions, both systems can be distinguished even if the spectral spacing between Pb I 405.68 nm and Fe I 406.35 nm is less than a nanometer.

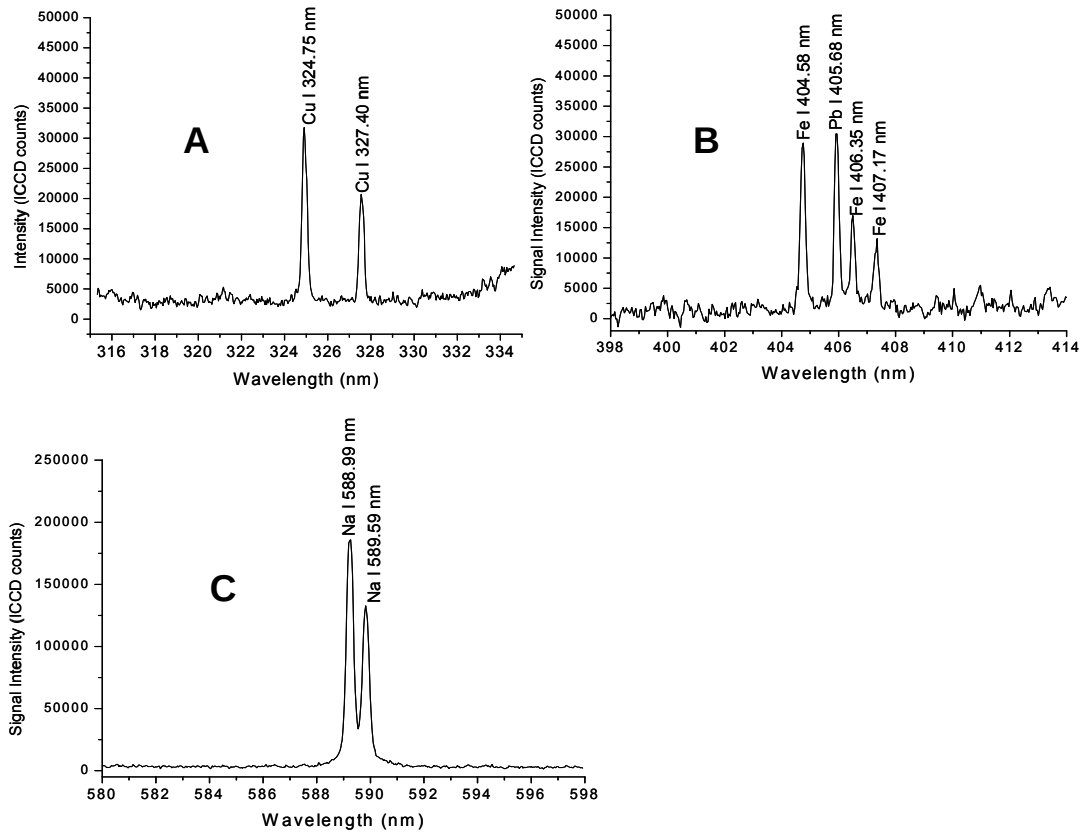

Figure 9: In figure 8, the regions referred to as A, B and C are enlarged for clarity. A corresponds to Cu I, B corresponds to Fe I and Pb I and C corresponds to Na I.

Similar to our previous experiment on sodium, we measured the different detection limits of the various compounds. In this measurement, the fog concentration is, once again, characterized over 120 cm with a 95 % transmission of the 632 nm He-Ne laser light. The characterizations were accomplished with respect to the 324.75 nm, 404.58 nm, 405.68 nm and 589 nm atomic transitions for $CuCl_2$, $FeCl_2$, $PbCl_2$ and NaCl respectively (36). For each salt, the solution was prepared individually and the concentration was varied and plotted against the signal intensity for a given line. Because the plotted curves behaved linearly, we could find the detection limit of the method for the various compounds using a

linear extrapolation to the 3σ level (where σ is the standard deviation of the signal). The detection limits were respectively, for $FeCl_2$, $CuCl_2$, $PbCl_2$ and NaCl, 0.001 mol/L_{water} (127 mg/L_{water}), 0.0002 mol/L_{water} (27 mg/L_{water}), 0.00003 mol/L_{water} (9 mg/L_{water}) and 0.00005 mol/L_{water} (3 mg/L_{water}). For these thin fog conditions, the detection limit for lead is the lowest.

An unexpected interesting result emerged from this aerosol concentration analysis. It was found that H I emissions varied with the solution concentration. To illustrate the phenomenon, figure 10 shows the plot of the signal from H I 656 nm as a function of the $FeCl_2$ solution's concentration. It appears that the atomic hydrogen emissions are enhanced when the salt's concentration is increased. Since this behavior has also been observed with all the other studied components, this increase signal is not due to a contribution from the weak fluorescence lines of Fe I located around 656 nm.

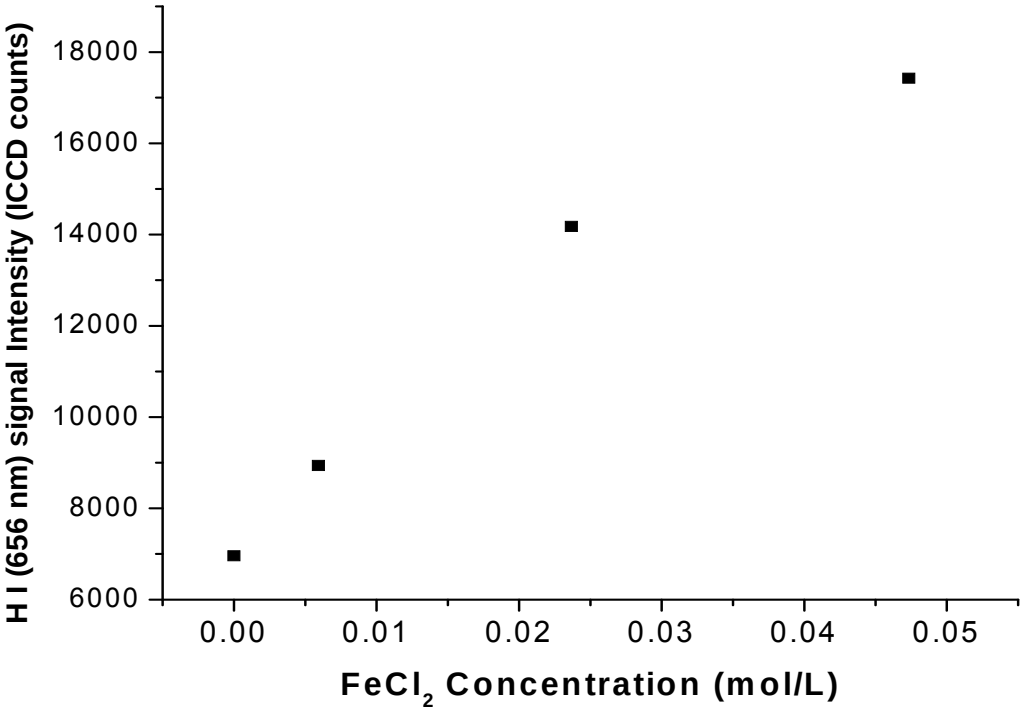

Figure 10: Variation of the H I (656 nm) fluorescence signal as a function of the concentration of the iron dichloride's solution.

In fact, because of the rather long pulses used in this experiment (500 fs negatively chirped), avalanche ionization (27) plays a non-negligible role in the interaction and explains the previously enhanced hydrogen signal. Indeed, longer pulses have a longer time to heat and accelerate electrons through inverse Bremsstrahlung effect. These accelerated electrons with high enough kinetic energy will ionize other atoms through subsequent collisions and release more electrons. The latter will undergo again the same inverse Bremsstrahlung processes and generate more electrons through the cascade (avalanche) ionization process. This would increase the ionization efficiency of the H_2O molecules. The presence of the dissolved salts enhances this effect by introducing inside the droplet, chlorine ions with weakly bonded electrons. As a consequence, it will be easier

for the laser pulse to liberate these electrons and enhance the avalanche effect. Like every other cascaded effects, avalanche ionization is strongly dependent on the initial conditions. Consequently, these supplementary electrons would strongly influence the ionization process and as shown on figure 10, leading to huge hydrogen signal increase. The above observation also suggests that avalanche ionization of the aerosol is the main interaction mechanism that results in the generation of the plasma. Electron-ion recombination would lead with the eventual emission of the various fluorescence signals.

6. Conclusion

Based upon the above results, we will try to answer the following question: Can R-FIBS be efficiently used in real applications of remote detection of aerosols? To do so, we will analyze and interpret the obtained results to determine whether or not R-FIBS meets the specified requirements mentioned at the beginning of this document.

With the first series of experiments on sodium, we demonstrated that remote sensing of aerosol clouds based on R-FIBS measurement can easily fulfill the first two requirements, namely, the possibility of remote detection at variable distances and sensitive to low concentrations. In fact, we experimentally demonstrated that aqueous aerosols containing traces of NaCl could be detected at a distance of 70 m from the LIDAR. Moreover, an extrapolation based on the LIDAR equation revealed that more energetic pulses could lead to kilometer range detection. Because of the wide range of distances at which R-FIBS can be used, it represents a great candidate for probing aerosols in all three major scales: industry, atmospheric and military.

For the second criterion, sensitivity, all dissolved salts used for the experiments proved themselves as being easily observed at very low concentrations. At a 5 m distance, the detection limits on concentration ranged from 0.001 mol/L_{water} (127 mg/L_{water}) for $FeCl_2$ to 0.00003 mol/L_{water} (9 mg/L_{water}) for $PbCl_2$. All these values represent the quantity of salt contained in the water solution. However, from the 95 % transmission of the 632 nm wavelength, we calculated an approximate droplet concentration of 300 cm^{-3}. The rest of the volume is totally occupied by air at STP. As a consequence, laser pulses will interact

with a medium consisting of air and water spheres containing high density contaminants. According to the 'US environmental protection agency' (NAAQS, *National Ambient Air Agency*, see http://www.epa.gov/air/criteria.html), the tolerated standard concentration for respiratory exposure to airborne substances containing lead is 1.5 $\mu g_{Pb}/m_{air}^3$ (8). Let us consider our situation in which lead is found in liquid H_2O containing $PbCl_2$ at the limiting concentration of our detection. Under these conditions, the 5 µm radius droplet contains 16 x 10^{-20} moles of lead dichloride. With a droplet density of 300 000 L^{-1}, the lead concentration is approximately 1.4 $\mu g_{Pb} / m_{air}^3$. This is of the same order of magnitude as the tolerated concentration cited above. Thus, even though the above demonstration consists in a rough approximation, we can conclude that R-FIBS could potentially be efficiently used to detect such pollutants (lead) in industries and in other contaminated sites so as to prevent many unnecessary short and long term accidents caused by respiratory intoxications. We have performed the same exercise for the other constituents and we obtained the following concentration limits: 20 $\mu g_{Fe} / m_{air}^3$, 4.2 $\mu g_{Cu} / m_{air}^3$ and 471 ng_{Na} / m_{air}^3.

For many applications, such as air quality monitoring, the concentration of a single constituent has to be constantly known. However, applications such as atmospheric characterization involve droplets containing multiple unknown samples. In these cases, the system has to be able to recognize and distinguish the various components as stated in the third requirement for an 'ideal' detection. In fact, the simultaneous detection of multiple constituents can cause spectral overlap of the fluorescence lines which complicates the elemental recognition and distinction processes. In our experiment, the reported atomic fluorescence lines revealed by the low plasma density filaments did not show any overlap.

Four fluorescence lines can be observed and distinguished in a spectral domain as small as 2 nm (figure 9B). Also, two fluorescence peaks spectrally separated by 0.6 nm can easily be resolved (figure 9C). These unique properties of the technique demonstrate the great sensitivity and selectivity of R-FIBS in aerosol for recognition and distinction purposes.

In conclusion, we experimentally demonstrated that R-FIBS is a sensitive and selective technique to probe the composition of a distant aerosol cloud. The extreme laser efficiency to excite the dissolved ions proves that any metals having a strong atomic fluorescence transition between 300 nm and 800 nm can be detected with our instrument. Because of this property, the possibility of observing many atmospheric constituents of interest is not to be questioned anymore. For a toxic material such as Hg that has a visible atomic transition line that is much stronger than Pb I, Hg fluorescence using R-FIBS should be excited and detected efficiently. Moreover, each of the dissolved atoms revealed a unique and characteristic fluorescence trace that could be distinguished from the others. From the four constituents in solution, 41 atomic transitions were reported without any spectral overlap. Because of the distance criterion, R-FIBS is not yet ready for multi kilometer applications; more long range experiments have to be carried out. However, the obtained results show that for applications such as industrial security, large city smog characterization and industrial chimney control, R-FIBS can efficiently be used.

7. References

1. **Borrmann, S., and J. Curtius.** Lasing on a cloudy afternoon. *Nature.* 2002, 418, pp. 826-827.

2. **J. -R. Simard, G. Roy, P. Mathieu, V. Larochelle, J. McFee, J. Ho.** *Standoff detection of bioaerosols from laser-induced fluorescence.* Valcartier : DRDC, 2002. p. 113. DREV-TR-2002-125.

3. **K. Stelmaszczyk, P. Rohwetter, G. Méjean, J. Yu, E. Salmon, J. Kasparian, R. Ackermann, J.-P. Wolf, and L. Wöste.** Long-distance remote laser-induced breakdown spectroscopy using filamentation in air. *Applied Physics Letters.* 2004, 85, p. 3977.

4. **Svanberg, S.** *Air Monitoring by Spectroscopic Techniques.* [ed.] M.W. Sigrist. New York : Wiley, 1994.

5. **(CSST), Commission sur la Santé et la Sécurité au Travail.** Service du répertoire toxicologique. [Online] 2008. http://www.reptox.csst.qc.ca/.

6. **J.H. Seinfeld, S.N. Pandis.** *Atmospheric Chemistry and Physics: from Air Pollution to Climate Change.* New York : Wiley, 1998.

7. **Institue, The Franklin.** Aeronautic Internet Textbook. [Online] 2008. http://www.fi.edu/wright/again/wings.avkids.com/wings.avkids.com/Book/Atmosphere/instructor/clouds- 01.html.

8. **agency, US environmental protection.** Air and radiation. *National Ambient Air Agency.* [Online] 2008. [Cited:]

9. **Park, C.B. Song and H.S.** Analytic solutions for filtration of polydisperse aerosols in fibrous filter. *Powder technologies.* 2006, 170, pp. 64–70.

10. **H.L. Xu, G. Méjean, W. Liu, Y. Kamali, J.-F. Daigle, A. Azarm, P.T. Simard, P. Mathieu, G. Roy, J.-R. Simard, S.L. Chin.** Remote sensing of similar biological materials

using femtosecond filament-induced breakdown spectrocospy. *Applied Physics B.* 2007, 87, p. 151.

11. **H.L. Xu, Y. Kamali, C. Marceau, P.T. Simard, W. Liu, J. Bernhardt, G. Méjean, P. Mathieu, G. Roy, J.-R. Simard, S.L. Chin.** Simultaneous detection and identification of multigas pollutants using filament-nduced nonlinear spectroscopy. *Applied physics letters.* 2007, 90, pp. 101-106.

12. **B.C Windom, P.K. Diwakar, D.W. Hahn.** Dual-Pulse LIBS for Analysis of Gaseous and Aerosol Systems. *Spectrochimica Acta Part B.* 2006, 61, pp. 788–796.

13. **S.L. Chin, S.A. Hosseini, W. Liu, Q. Luo, F. Théberge, N. Aközbek, A. Becker, V.P. Kandidov, O.G. Kosareva, and H. Schroede.** The propagation of powerful femtosecond laser pulses in optical media: physics, applications, and new challenges. *Canadian journal of physics.* 2005, 83, pp. 863-905.

14. **A. Becker, N. Akozbek, K. Vijayalakshmi, E. Oral, C.M. Bowden, S.L.Chin.** Intensity clamping and re-focusing of intense femtosecond laser pulses in nitrogen molecular gas. *Applied physics B.* 2001, 73, pp. 287-290 .

15. **G. Méchain, A. Couairon, Y.-B. André, C. D'Amico, M. Franco, B. Prade, S. Tzortzakis, A. Mysyrowicz, R. Sauerbrey.** Long range self-channeling of infrared laser pulses in air: a new propagation regime without ionization. *Applied Physics B.* 2004, 79, pp. 379–382.

16. **W. Liu, F. Theberge, J.-F. Daigle, P.T. Simard, S.M. Sarifi, Y. Kamali, H.L. Xu, S.L. Chin.** An efficient control of ultrashort laser filament location in air for the purpose of remote sensing. *Applied Physics B.* 2006, Vol. 85, 1, p. 55.

17. **Francis Théberge, Weiwei Liu, Patrick Tr. Simard, Andreas Becker, See Leang Chin.** Plasma density inside a femtosecond laser filament in air: Strong dependence on external focusing. *Physical Review E.* 2006, 74, p. 036406.

18. **H.L. Xu, W. Liu, S. L. Chin.** Remote time-resolved filament-induced breakdown spectroscopy of biological materials. *Optics Letters.* 2006, 31, pp. 1540-1542.

19. **H.L. Xu, J.F. Daigle, Q. Luo, S.L. Chin.** Femtosecond laser-induced nonlinear spectroscopy for remote sensing of methane. *Applied Physics B.* 2006, 82, p. 655.

20. **Q. Luo, H.L. Xu, S.A. Hosseini, J.-F. Daigle, F. Theberge, M. Sharifi, S.L. Chin.** Remote sensing of pollutants using femtosecond laser pulse fluorescence spectroscopy. *Applied Physics B.* 2006, 82, pp. 105-109.

21. **G. Méjean, J. Kasparian, J. Yu, E. Salmon, S. Frey, J.-P. Wolf, S. Skupin, A. Vinçotte, R. Nuter, S. Champeaux, and L. Bergé.** Multifilamentation transmission through fog. *Physical review E.* 2005, 72, p. 026611 .

22. **Riad Bourayou, Guillaume Méjean and Jérôme Kasparian, Miguel Rodriguez, Estelle Salmon and Jin Yu.** White-light filaments for multiparameter analysis of cloud microphysics. *Journal of the Optical Society of America B.* 2005, Vol. 22, 2, pp. 369-377.

23. **François Courvoisier, Véronique Boutou, Jérôme Kasparian, Estelle Salmon, Guillaume Méjean, Jin Yu, and Jean-Pierre Wolf.** Light Filaments Transmitted through Clouds. *Applied Physics Letters.* 2003, 83, p. 2.

24. **G. Méjean, J. Kasparian, J. Yu, S. Frey, E. Salmon, and J.-P. Wolf.** Remote detection and identification of biological aerosols using a femtosecond terawatt lidar system. *Applied Physics B.* 2004, 78, p. 535.

25. **Takashi Fujii, Naohiko Goto, Megumu Miki, Takuya Nayuki, and Koshichi Nemoto.** Lidar measurement of constituents of microparticles in air by laser-induced

breakdown spectroscopy using femtosecond terawatt laser pulses. *Optics Letters.* 2007, Vol. 31, 23, pp. 3456-3458.

26. **Encyclopedia, Wikipedia Free.** Dead sea. [Online] 2007. http://en.wikipedia.org/wiki/Dead_Sea.

27. **Chin, S. L.** From Multiphoton to Tunnel Ionization. [ed.] A. A. Villaeys and Y. Fujimura S. H. Lin. *Advances in Multiphoton Processes and Spectroscopy.* Singapore : World Scientific, 2004, 16, pp. 249 - 272 .

28. **Boyd, Robert W.** Chapter 7: Processes Resulting from Intensity Dependent Refractive Index. *Nonlinear Optics.* USA : Elsevier sciences, 2003, pp. 311-324.

29. **A. Braun, G. Korn, X. Liu, D.Du, J. Squier, G Mourou.** Self-channeling of high-peak-power femtosecond laser pulses in air. *Optics Letters.* 1995, 20, p. 73.

30. **H.R. Lange, A. Chiron, J.-F. Ripoche, A. Mysyrowicz, P. Berger, P. Agostini.** High-Order Harmonic Generation and Quasiphase Matching in Xenon Using Self-Guided Femtosecond Pulses. *Physical review Letters.* 1998, 81, p. 1611.

31. **A Brodeur, C Y Chien, F A Ilkov, S L Chin, O G Kosareva & V P Kandidov.** Moving focus in the propagation of powerful ultrashort laser pulses in air. *Optics Letters.* 1997, 22, pp. 304-307.

32. **Marburger, J.H.** Theory of self focusing. *Progress Quantum Electronics.* 1975, 4, p. 35.

33. **S.A. Hosseini, Q. Luo, B. Ferland, W. Liu, S.L. Chin, O.G. Kosareva, N.A. Panov, N. Aközbek, V.P. Kandidov.** Competition of multiple filaments during the propagation of intense femtosecond laser pulses. *Physical review A.* 2004, 70, p. 033802.

34. **Q. Luo, S.A. Hosseini, W. Liu, J.-F. Gravel, O.G. Kosareva, N.A. Panov, N. Aközbek, V.P. Kandidov, G. Roy and S.L. Chin.** Effect of beam diameter on the propagation of intense femtosecond laser pulses. *Appled Physics B.* 2005, 80, pp. 35-38.

35. **F. Théberge, W. Liu, Q. Luo, S. L. Chin.** Ultrabroadband continuum generated in air (down to 230 nm) using ultrashort and intense laser pulses. *Applied Physics B.* 2005, 80, pp. 221-225.

36. NIST atomic spectra database. *National Institute of standards and Technologies.* [Online] 2008. http://physics.nist.gov/PhysRefData/ASD/index.html.

37. **Satelites, Committee on Earth Observation.** resources in earth Observations. [Online] http://ceos.cnes.fr:8100/cdrom-98/astart.htm .

38. **A. Talebpour, M. Abdel-Fattah, A. D. Bandrauk & S. L. Chin.** Spectroscopy of the gases interacting with intense femtosecond laser pulses. *Laser Physics.* 2001, 11, pp. 68-76.

39. **A Talebpour, S. Petit & S.L. Chin.** Re-focusing during the propagation of a focused femtosecond Ti:Sapphire laser pulse in air. *Optics Communications.* 1999, 171, pp. 285-290.

40. Cumulus Humilis Clouds. *Wikipedia Free Encyclopedia.* [Online] http://en.wikipedia.org/wiki/Cumulus_humilis_cloud.